Talanta 266 (2024) 124941

Contents lists available at ScienceDirect

Talanta

journal homepage: www.elsevier.com/locate/talanta

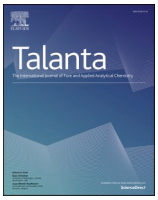

Extending the range of metal ions SERS detection using hybrid plasmonic/ZIF-8 particles

Nicolas Pazos-Perez, Luca Guerrini *

Department of Physical and Inorganic Chemistry, Universitat Rovira I Virgili, Carrer de Marcel•lí Domingo 1, 43007, Tarragona, Spain

ARTICLE INFO

Handling Editor: A Campiglia

Keywords:
Surface-enhanced Raman spectroscopy
Plasmonic nanoparticles
Metal ions
Detection
Metal-organic frameworks (MOFs)
Wilson's disease

ABSTRACT

Nanosensors based on surface-enhanced Raman spectroscopy (SERS) have emerged as a class of promising optical tools for the ultrasensitive quantification of metal ions of environmental and biological interest. A central bottleneck in this field is the availability of suitable surface receptors able to convert the selective binding with these vibrationless analytes into measurable SERS signals. In this work, we tackle this issue by employing a hybrid substrate comprising a highly SERS-active plasmonic core and a ZIF-8 metal-organic framework (MOF) shell. The ZIF-8 shell firmly captures aromatic receptors close to the plasmonic structure regardless of their intrinsic affinity for the metallic surface and without altering their ability to coordinate metal ions. Furthermore, it imparts molecular sieving abilities enabling the direct use of the SERS sensing platform in complex media such as biological fluids. This was demonstrated by using different classes of chromogenic reagents (bathocuproine, a 2,6':2′,2″-terpyridine derivative, and Arsenazo III) which were exploited for the SERS detection of both transition and alkaline earth metal ions (i.e., divalent copper, cobalt and calcium ions). Notably, we successfully applied this approach for the detection of Cu(II) in untreated urine samples for Wilson's disease diagnosis. Overall, we believe this class of multifunctional hybrid substrates will serve as a valuable material for expanding the applicability of SERS spectroscopy in real-life environmental and biomedical metal ions analysis.

1. Introduction

Metal contamination, especially that resulting from transition metals, has been causing increasing ecological and public health concerns due to the growing human exposure to dangerous levels of these non-biodegradable elements [1,2]. The specific chemical nature of each metal element determines the resulting toxicological impact and, thus, both tolerated dose and exposure time [1,2]. For instance, guidelines for drinking water quality released by World Health Organization, the European Union, and the Environmental Protection Agency recommend acceptable concentrations of copper, cobalt, and mercury in the 1.3–2 mg/L, 20–200 μg/L and 1–6 μg/L ranges, respectively [2].

On the other hand, metal ions are also fundamental elements in many biochemical reactions and cell functioning. As the homeostasis of metal ions (e.g., iron, copper, zinc, and calcium) is required for maintaining normal physiological functions, abnormal levels of these species are responsible for the emergence of many diseases (e.g., carcinogenesis, and neurodegenerative and growth disorders) [3–6]. A paradigmatic example is represented by Wilson's Disease (WD), a genetic disorder leading to an accumulation of copper in various body tissues [7]. If left untreated, WD leads to progressive liver and neurological dysfunction and, eventually, death [8]. Thus, early diagnosis is central for improving the patient's prognosis but it is often challenged by the lack of specific symptoms [7]. As a result, the quantification of copper in biofluids became an important analytical tool for WD diagnosis [7,8].

Overall, the central roles of metal ions as environmental pollutants as well as in biology and medicine make the quantification of these species an extremely active and interdisciplinary field of research. Established analytical methods typically rely on spectroscopic techniques such as atomic absorption (AAS) and atomic emission (inductively coupled plasma, ICP) which, when respectively coupled to a graphite furnace (GFAAS) or a mass detector (ICP-MS), can afford limits of detection in the ppb/ppt levels [9]. However, these techniques are often expensive and destructive, require large volumes of samples, or employ toxic gases. Most remarkably, these methodologies cannot be implemented remotely, thus requiring the samples to be stored and, typically, pre-treated before analysis which can eventually lead to analyte losses and sample alterations [10]. As a result, there has been an increasing

* Corresponding author.
E-mail address: luca.guerrini@urv.cat (L. Guerrini).

https://doi.org/10.1016/j.talanta.2023.124941
Received 17 May 2023; Received in revised form 4 July 2023; Accepted 11 July 2023
Available online 16 July 2023

interest in developing novel optical methods to address the limitations of conventional approaches [11–14]. Notably, the synergistic combination of optical methods with the extraordinary properties of nanoscale materials has been paving the way for the design and fabrication of highly sensitive, versatile, and specific nanosensors [15–17].

In this regard, surface-enhanced Raman spectroscopy (SERS) has emerged as one of the most intriguing nanoscale analytical techniques [18,18–21]. Indeed, SERS exploits the excitation of localized surface plasmon resonances (LSPRs) at nanostructured metallic substrates to largely amplify the Raman signals from molecular scatterers located in their close proximity. In recent years, the focus has been put on integrating SERS into multifunctional systems to facilitate the transition from basic proof-of-concept studies on simple artificial matrices to routine analysis of real-life samples [15,22,23]. For instance, within the field of SERS-based metal ion detection, multidisciplinary strategies have been developed to engineer a diverse range of hybrid platforms (e.g., capillary, microfluidic, magnetic, and paper-based SERS sensors) affording sample handling, processing capabilities (e.g., filtration, pre-concentration, and separation) and miniaturized system for remote analysis [15,22–25]. Notably, a pivotal aspect in the design of a SERS platform for the quantification of vibrationless analytes is the availability of appropriate molecular receptors (i.e., chemoreceptors) to be used as SERS transducers. In this context, the chemoreceptor simultaneously (i) interacts with the analyte and (ii) provides an intense SERS spectrum that undergoes major spectral changes upon interaction with the target, thereby converting the selective binding to metal ions into measurable SERS signals [25,26]. Combining into a single molecular entity these two functions improves the robustness of the sensor response while reducing the complexity of its design since chemosensors can intrinsically provide an internal standard for ratiometric SERS analysis [25]. For the most part, chemoreceptors are chosen among those equipped with a mercapto or disulfide group can firmly attach the metallic surfaces via formation of the strong metal-sulfur bond [25,27]. It is not surprising, then, that the large majority of metal ion SERS sensing studies reported in the literature focused on the determination of Hg(II). On the one hand, mercury contamination is a major public health and environmental problem; on the other, various selective thiolated chemoreceptors for Hg(II) are commercially available or amenable to simple chemical synthesis and *a la carte* modifications (e.g., thymine-rich aptamers) [28,29]. In principle, the classical qualitative colorimetric analysis can offer an untapped wealth of potential SERS chemoreceptors for selective discrimination of inorganic species that could significantly increase the number of possible targets, facilitate multiplex detections, and even enable speciation analysis. However, their exploitation in SERS has been considerably restricted mainly by (i) the impossibility or difficulty of equipping the receptor with mercapto/disulfide groups and/or (ii) the direct binding to the metallic substrate via the same functional groups that are involved in the coordination to the inorganic target, a condition that suppresses their function as chemoreceptors [25]. Our group previously demonstrated that this issue can be partially circumvented by exploiting the intercalative binding of small aromatic ligands into duplex oligonucleotides [30]. In this study, the intercalation of alizarin red S (ARS) into short double-stranded DNAs allowed for retaining the ARS chelation capabilities toward Fe(III) and Al(III) which we exploited to detect these ions in spiked tap water using DNA-modified silver nanoparticle clusters [30]. However, this strategy is viable only for those molecules that efficiently intercalate between duplex base pairs while, at the current stage, this approach is also restricted to the use of positively-charged colloids as plasmonic substrates.

Metal-organic frameworks (MOF) are inorganic–organic hybrid crystalline materials exhibiting ultrahigh and very defined porosity which are formed by the coordination of organic linkers and metal nodes [31]. Further, the physicochemical properties of MOFs can be tuned by changing the organic ligand and/or the inorganic cation units. These characteristics make MOFs excellent candidates to be combined with plasmonic nanostructures [31–39] as they provide to the plasmonic counterparts with chemical and size selectivity as well as enhanced thermal, chemical, and colloidal stability [31,33,36]. In this regard, we have very recently described the fabrication of a novel multifunctional sensing platform comprising highly SERS-active silver nanoparticles (AgNPs)-decorated polystyrene beads (PS) wrapped within a shell of zeolitic imidazolate framework (ZIF-8) to yield hybrid microparticles (referred to as PS@AgNPs@ZIF-8) [40]. The high adsorption capacity of ZIF-8 has been exploited to firmly entrap bathocuproine (BC), a well-known chromogenic reagent for the colorimetric analysis of copper species [41,42], and the resulting SERS sensing system was successfully used for Cu(II) quantification in freshwaters [40].

Herein, we first build on this recent finding to demonstrate the great analytical potential of this class of particles as a low-cost Wilson Disease diagnosis tool via rapid SERS detection of Cu(II) in unprocessed human urine samples. Secondly, we assess the nature of the hybrid plasmonic particles as flexible carriers for a diverse range of conventional organic chemoreceptors to be used in the SERS detection of different classes of metal ions. We believe that this constitutes a major finding for bolstering the analytical application of SERS in metal ion sensing in real-life environmental and biomedical samples.

2. Materials and methods

2.1. Materials

Silver nitrate (99%, $AgNO_3$), L-ascorbic acid (99%, AA), sodium citrate tribasic dihydrate (≥98%), zinc acetate dihydrate (98%, $Zn(CH_3COO)_2{\cdot}2H_2O$), 2-methylimidazole (2-MeIm, 99%, $C_4H_6N_2$), poly (allylamine hydrochloride) (PAH, MW = 15,000 Da), sodium chloride (≥99.5%, NaCl), potassium chloride (≥99%, KCl), sodium phosphate dibasic (≥99%, Na_2HPO_4), sodium phosphate monobasic (≥99%, NaH_2PO_4), cobalt(II) nitrate hexahydrate (98%, $Co(NO_3)_2{\cdot}6H_2O$), copper(II) chloride dihydrate (≥99%, $CuCl_2{\cdot}2H_2O$), calcium chloride dihydrate (≥99%, $CaCl_2{\cdot}2H_2O$) and ethanol (99.5%) were purchased from Sigma-Aldrich (Germany). Bathocuproine (98%, BC), and 4'-(4-bromophenyl)-2,6':2′,2″-terpyridine (98%, p-tpy) were purchased from Fisher Scientific. Polystyrene bead solution (~500 nm diameter, AJ50) was purchased from Ikerlat Polymers (Spain). Hexadecyltrimethylammonium bromide (CTAB) (≥99%) was purchased from Acros Organics (Germany). All reactants were used without further purification. Milli-Q water (18 MΩ cm^{-1}) was used in all aqueous solutions, while all glassware was cleaned with aqua regia before the experiments.

2.2. Synthesis of silver nanoparticles (AgNPs)

Silver colloids were prepared as previously described [43]. An aqueous mixture of ascorbic acid (100 μL, 0.1 M) and sodium citrate tribasic dihydrate (1.364 mL, 0.1 M) was added under strong magnetic stirring to 100 mL of boiling water. 1 min later, a mixture of 0.1 M $AgNO_3$ (298 μL) and 0.1 M $MgSO_4$ (224 μL), previously incubated for 5 min, was added to the boiling solution. After additional 30 min boiling, the sample was left to cool down at room temperature and, then, submitted to one centrifugation-washing cycle (6500 rpm, 15 min) to remove the excess of citrate molecules from the medium. The pellet was finally redispersed in Milli-Q water (final Ag^0 concentration = 1.4 mM).

2.3. AgNPs assembly on polystyrene beads (PS@AgNPs)

Firstly, polystyrene beads (PS) of ~500 nm diameter were coated with a positively charged polymer (PAH) as described as follows. 10 mg of PAH were added to 10 mL of NaCl aqueous solution (0.5 M). The mixture was sonicated for 30 min before being combined with 100 μL of PS bead solution (100 mg/mL). The sample was stirred for 30 min at 500 rpm and, then, submitted to three centrifugation-washing cycles

(10500 rpm, 30 min) with Milli-Q water to remove unbound PAH molecules. The resulting PS@PAH beads were redispersed in 50 mL of Milli-Q water (PS concentration = 0.2 mg/mL). To this sample, 10 mL of Ag colloids ([Ag^0] = 1.4 mM) were added dropwise under sonication. The mixture was immediately stirred (300 rpm) for another 30 min. Three centrifugation-washing cycles (4500 rpm, 15 min) with Milli-Q water were carried out to remove unbound AgNPs from the medium. The so-formed PS@AgNP beads were redispersed in 10 mL of Milli-Q water (PS concentration = 1 mg/mL).

2.4. Synthesis of ZIF-8 coated PS@AgNP beads (PS@AgNP@ZIF-8)

PS@AgNP@ZIF-8 particles were prepared as previously described [40]. Briefly, 3 mL of PS@AgNP suspension (1 mg/mL) were combined with 157.9 μL of a 10 mM CTAB aqueous solution (final CTAB concentration = 0.5 mM). 3 mL of 2-MeIm aqueous solution (1.32 M) were then added under stirring (500 rpm). 10 min later, 3 mL of $Zn(CH_3COO)_2$ aqueous solution (24 mM) were also added under stirring. After 5 minutes, the stirring was interrupted and the sample was left to incubate at room temperature for 3 h. Afterward, the sedimented PS@AgNP@ZIF-8 particles were separated from the whitish supernatant and redispersed in 10 mL of Milli-Q water (pH 7.8). Two centrifugation-washing cycles (4500 rpm, 5 min) were performed to selectively remove pristine ZIF-8 particles. The PS@AgNP@ZIF-8 pellet was finally redispersed in 50 mL of Milli-Q water (pH 7.8, PS concentration = 0.2 mg/mL).

2.5. Sample preparation for SERS analysis

500 μL of PS@AgNP@ZIF-8 (0.2 mg/mL) were added to 10 mL of an ethanolic solution of bathocuproine (BC, 10 μM), 4'-(4-bromophenyl)-2,6':2′,2″-terpyridine (p-tpy, 10 μM), or Arsenazo III (AZ, 100 μM). The mixtures were incubated overnight and then submitted to two centrifugation-washing cycles (4500 rpm, 5 min) with Milli-Q water (pH 7.8). The chromophore-loaded PS@AgNP@ZIF-8 particles were finally redispersed in 1 mL of Milli-Q water (pH 7.8). An identical protocol was applied for PS@AgNP particles when indicated. For metal ion detection, 100 μL of chemoreceptor-loaded PS@AgNP@ZIF-8 particles (PS concentration = 0.2 mg/mL) were added to 1 mL of sample. Samples of aqueous solutions of metal ions at different concentrations were prepared in PBS buffer (pH 7.8) or by spiking urine samples. Urine was acquired from a healthy volunteer for 24 h and stored in a copper-free bottle, following the methodology of traditional clinical tests that quantify the levels of 24 h urinary copper excretion [8].

2.6. Instrumentation

Material characterization was performed using UV–Vis spectroscopy (Agilent Technologies, Cary 8454), transmission electron microscopy (JEOL JEM 1010, operating at an acceleration voltage of 100 kV), ζ potential (Malvern Zetasizer Nano ZS). SERS spectra were acquired on colloidal suspensions using a Renishaw inVia Reflex system equipped with a 2D-CCD detector, a Leica confocal microscope, and a 532 nm frequency doubled Nd:YAG/Nd:YVO4 diode laser. A macrolens was used to focus the laser on the sample (power at the sample = 17.1 mW, exposure time = 10 s, accumulations = 3).

3. Results and discussion

Scheme 1 outlines the key features of substrate fabrication and sensing application in complex aqueous media. The hybrid plasmonic/ZIF-8 particles (PS@AgNP@ZIF-8) were prepared as previously described [40]. Firstly, positively-charged PS beads (~500 nm diameter) coated with poly(allylamine hydrochloride) were decorated with negatively-charged silver nanoparticles (AgNPs, ~50 nm diameter) via electrostatic assembly to yield PS@AgNPs materials (Fig. 1A and B). The assemblies were then redispersed into a cetyltrimethylammonium bromide (CTAB) aqueous solution to promote the formation of the surfactant double layer at the metallic interface. Such surface modification is critical to facilitate the subsequent direct growth of a well-defined single-crystalline ZIF-8 outer shell (Fig. 1A, C) [44]. The final PS@AgNPs@ZIF-8 hybrid particles (~850 nm diameter) exhibit a positive ζ potential (+17 mV) and a surface area (S_{BET}) of ~1000 m^2/g [40].

3.1. Quantification of Cu(II) in unprocessed human urine for Wilson's disease diagnosis

Nitrogen-containing ligands are major components in coordination chemistry as they profit from the lone pair electrons of aromatic nitrogens to coordinate with various transition metal cations [45]. For instance, cuproine molecules are well-known reagents for copper detection [42]. Among those, bathocuproine (BC), especially in its water-soluble form bathocuproine disulphonate, has been extensively

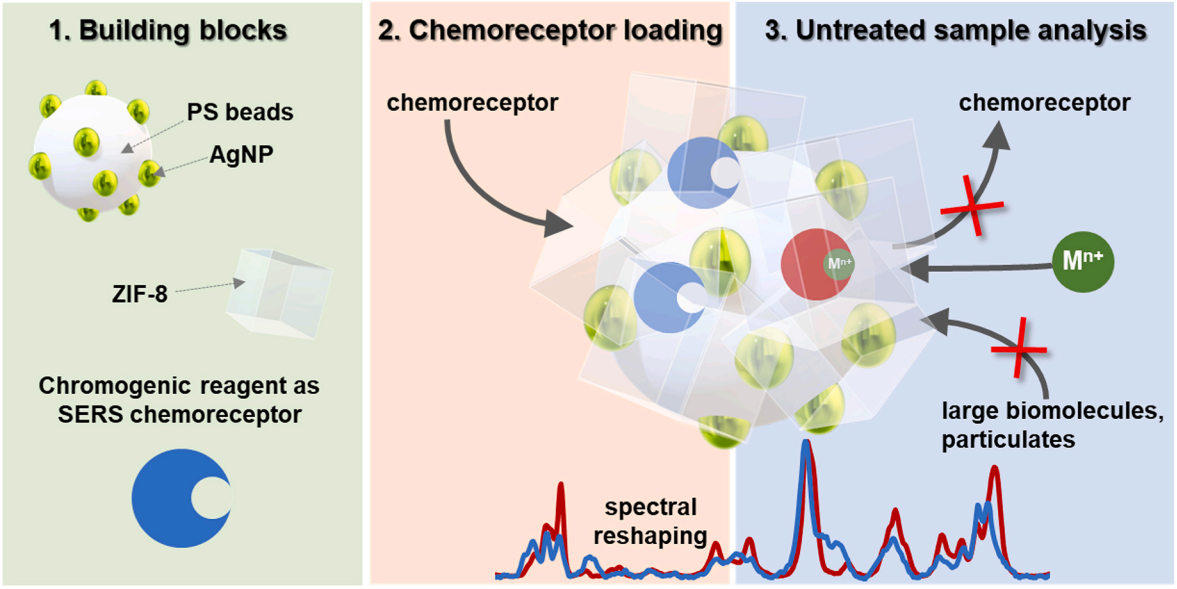

Scheme 1. Outline of the main features of the hybrid plasmonic/MOF particles (PS@AgNPs@ZIF-8) and their application in metal ion detection in complex aqueous media using conventional non-thiolated chromogenic reagents as SERS chemosensors.

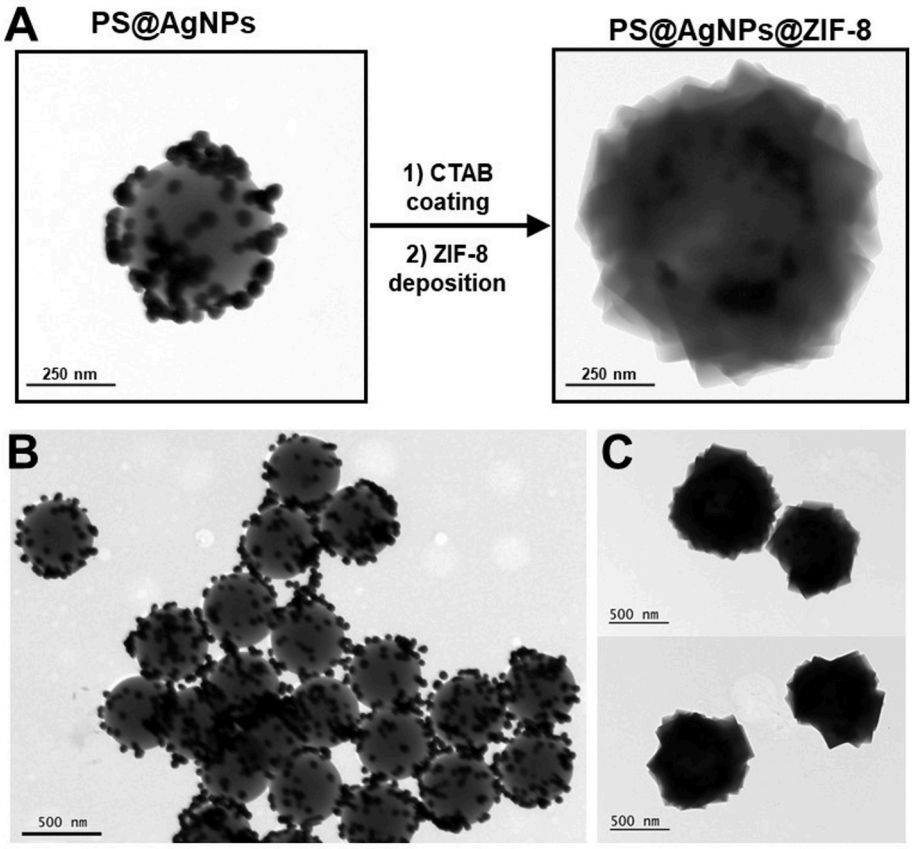

Fig. 1. Representative TEM images of (A, B) PS@AgNP and (A, C) PS@AgNP@ZIF-8 particles.

used as a highly specific colorimetric ligand for Cu(I) and Cu(II) [41,42]. As the nitrogen atoms of two BC molecules coordinate copper ions forming a metal ion complex, major alterations in the photophysical properties of the ligand occur, as revealed by the reshaping of its electronic absorption profile (Fig. 2A). In the same fashion, SERS spectra of BC-loaded on PS@AgNPs@ZIF-8 have shown to undergo extensive changes upon Cu(II) chelation [40]. In particular, the intensities of the spectral features centred at 1375 and 1424 cm^{-1}, ascribed to in-plane ring vibrations involving N–C stretching and CCH bending modes [46], were selected as spectral markers for ratiometric (I_{1424}/I_{1375}) quantification of copper ions, with a limit of detection of ~20 nM in PBS (pH 7.4) [40]. This has shown that the specificity for copper ion binding of BC molecules sequestered in the MOF shell of PS@AgNPs@ZIF-8 is maintained.

Primary biochemical investigations for Wilson's Disease (WD) diagnosis include urine tests that quantify urinary copper excretion during 24 h [8]. Thus, ~1 L of urine (pH 7.0) was collected from a healthy volunteer for 24 h in a copper-free container. Known amounts of $CuCl_2$ were then spiked in different urine aliquots to achieve the range of concentrations that is clinically relevant for WD diagnosis (from 0.1 μM to 4 μM). Currently, free Cu(II) levels above 0.6 μmol/24 h are considered strongly indicative of the disease while 1.6 μmol/24 h is the cut-off value for diagnosis [7,47]. SERS spectra of BC-loaded PS@AgNPs@ZIF-8 in human urine samples spiked with Cu(II) are illustrated in the spectral range of interest in Fig. 2B. Differently to freshwater samples [40], the urine matrix originates an extensive fluorescence background upon excitation with a 532 nm laser (Fig. S1) which, however, does not prevent the acquisition of intense and well-defined SERS features after baseline correction (Fig. 2B). The corresponding I_{1424}/I_{1375} values as a function of the spiked Cu(II) content are plotted in Fig. 2C and compared with those extracted from the identical target concentrations in PBS (pH 7.4). As it can be observed, very minor discrepancies are detected indicating the ability of BC-loaded PS@AgNPs@ZIF-8 to retain the sensing performance even in such a complex medium. We ascribed this remarkable feature to the ZIF-8 microporosity that prevents large biomolecules (e.g., proteins) and particulates to interact with the inner silver nanoparticles while permitting the rapid diffusion of small cations across the outer shell (i.e., molecular sieving properties) [48,49]. The ability of the ZIF-8 shell to act as an integrated filter obviates the need for a pre-filtration step upon sample collection, which is typically performed in trace analysis of heavy metal ions via conventional analytical methods to remove interfering particulates (e.g., ion chromatography, colorimetry, ICP-MS, ICP-AES, flame ASS, and graphite furnace ASS). Notably, in the absence of the outer ZIF-8 shell, no SERS signal of BC can be detected on PS@AgNPs, further highlighting the key role of the MOF shell in mantaining the organic ligands close to the plasmonic surface.

This proof-of-concept study demonstrates the applicability of BC-loaded PS@AgNPs@ZIF-8 particles for the rapid, simple, and low-cost detection of free Cu(II) in unprocessed human urines to help in WD diagnosis. It must be stressed that the BC content on PS@AgNPs@ZIF-8 has been approximately optimized to yield intense SERS signals with a high signal-to-noise ratio, which improves the accuracy and robustness of the SERS response, while maintaining the ligand concentration sufficiently low to meet the specific sensitivity requirements for clinical testing. The same approach will be applied to each chemoreceptor investigated in this study.

3.2. Hybrid plasmonic/MOF particles as an efficient and flexible platform for the SERS detection of various metal ions using conventional chromogenic reagents

Intrigued by these very promising results, we decided to test the suitability of PS@AgNPs@ZIF-8 particles as a general platform for entrapping other types of organic ligands to be used as SERS

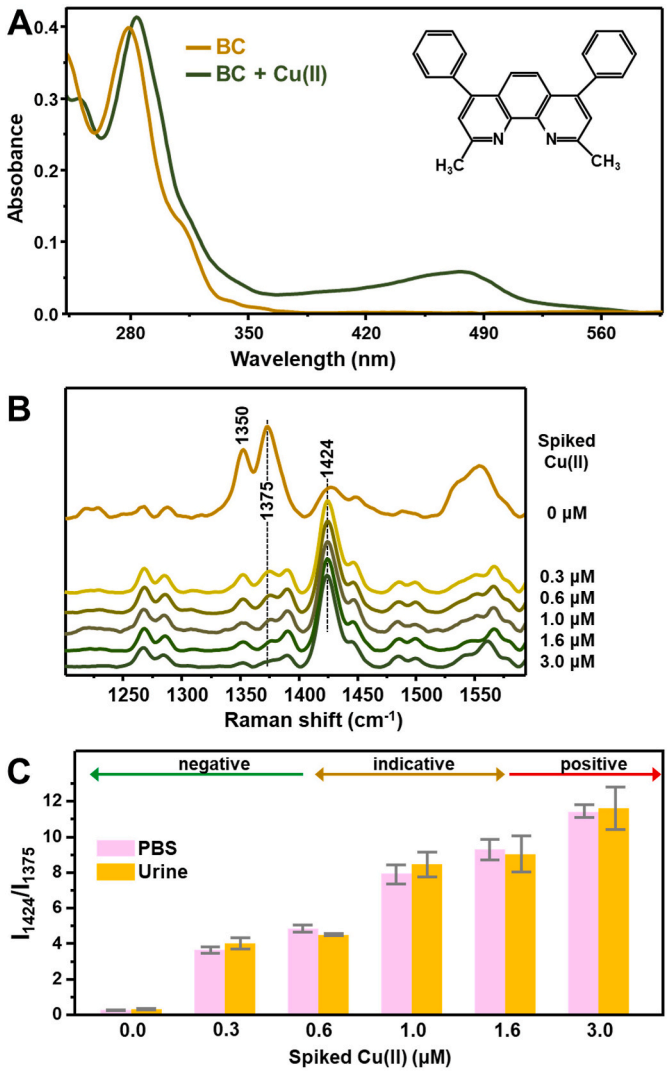

Fig. 2. (A) Absorption spectra of BC (10 μM) and BC + Cu(II) mixture (10 μM and 5 μM, respectively) in ethanol. The molecular structure of BC is also depicted. (B) SERS spectra of BC-loaded PS@AgNPs@ZIF-8 suspension in the 1200–1590 cm^{-1} spectral range upon immersion into urine samples spiked with different concentrations of Cu(II). (C) SERS intensities ratio I_{1424}/I_{1375} vs Cu(II) concentration for PBS (pH 7.8) and spiked urine samples.

chemoreceptors for metal ions detection. To this end, we selected two other classes of well-known commercially available metal-binding molecules: a 2,2′:6′,2″-terpyridine derivative and Arsenazo III.

2,2′:6′,2″-terpyridine (tpy) derivatives represent a class of N-containing ligands widely used in coordination chemistry. Notably, these NNN-tridentate ligands show a high affinity for first-row transition metal ions forming "closed-shell" octahedral tpy_2-M^{2+} complexes [45]. Upon metal ion coordination, tpy units adopt a nearly planar geometry transitioning from a *transoid* to a *cisoid* conformation [50]. The electronic structure of the tpy moiety in the metal complex depends strongly on the nature of the chelated species [50], which explains why the coordination with different metal ions causes distinct photophysical changes. In our previous work [51], these peculiar tpy properties were used to design a SERS-based method for the simultaneous determination of Cu(II) and Co(II). To this end, we have specifically synthesized a terpyridine derivative equipped with a dithiocarbamate (DTC) functionality introduced at the opposite side of the tpy moiety. Notably, the DTC derivatization of the synthetic tpy precursor was performed *in situ* and immediately before the mixing with silver colloids, due to the intrinsic instability of the DTC group. The introduction of the DTC functionality was required to promote both the strong binding to the silver surface via covalent Ag–S bonds and the adoption of a tilted orientation locating the pyridine units toward the bulk solution. Indeed, preventing the direct interaction of the active binding site with the plasmonic surface is critical for retaining the metal chelating capability of the receptor [30].

Herein, we selected 4'-(4-bromophenyl)-2,6':2′,2″-terpyridine (p-tpy, Fig. 3A) as a representative tpy ligand to demonstrate that complex synthetic procedures to equip such ligand with mercapto or

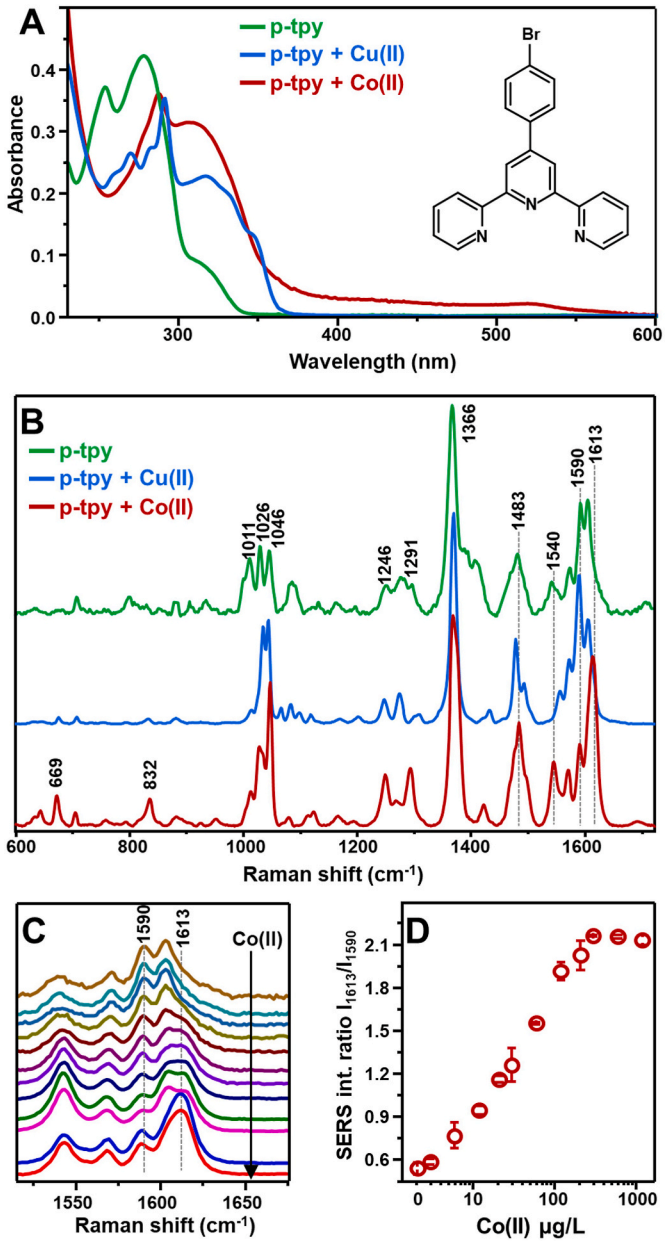

Fig. 3. (A) Absorption spectra of p-tpy and p-tpy + metal ions (10 μM and 20 μM, respectively) in ethanol. The molecular structure of 4-phenyl-2,6':2′,2″-terpyridine (p-tpy) is also depicted. (B) Normalized SERS spectra of p-tpy (5 μM) on PS@AgNPs@ZIF-8 upon immersion into 20 μM Cu(II) solution (1270 μg/L) or 20 μM Co(II) solution (1178 μg/L) in PBS buffer (pH 7.4). Spectra were arbitrarily normalized to the band at 1366 cm^{-1}. Excitation wavelength = 532 nm. (C) SERS spectra of p-tpy loaded PS@AgNPs@ZIF-8 suspension in the 1480-1700 cm^{-1} spectral range upon immersion into Co(II) solution in PBS buffer (pH 7.4) at different cobalt concentrations (from top to bottom: 0, 2.1, 2.9, 6.0, 12, 21, 29, 59, 118, 206, 294, and 589 μg/L). (D) SERS intensity ratio I_{1613}/I_{1590} vs. Co(II) concentration (N = 3).

dithiocarbamate functionalities are not necessary when the receptor is used in combination with PS@AgNPs@ZIF-8 particles. p-tpy is a widely commercially available chemical that can be produced in large batches with high purity [52]. Fig. 3A shows the absorption spectra of p-tpy and its Cu(II) and Co(II) complexes. Notably, the electronic spectrum of p-tpy comprises one group of bands arising from internal $\pi \rightarrow \pi^*$ transitions (below 400 nm) and a second set associated with charge-transfer transitions between the ligand and the specific chelated ion (400–700 nm) [53]. PS@AgNPs@ZIF-8 particles (0.1 mg) show the ability to fully capture p-tpy (50 nanomols) from a 5 μM ethanolic solution, as suggested by the absence of the ligand contribution from the optical spectrum of the collected supernatant (Fig. S2). The resulting SERS spectrum of p-tpy loaded PS@AgNPs@ZIF-8 particles (Fig. 3B) displays the characteristic vibrational pattern of 4-phenyl-2,6':2′,2″-terpyridine chemoreceptor [53]. Here, the set of bands can be broadly classified in the following spectral regions: (i) 500-950 cm^{-1}, mainly ascribed to δCH and δCCN vibrations; (ii) 950-1400 cm^{-1}, due to mixed contributions of νCC, νCN, and δCH modes; and (iii) 1400-1700 cm^{-1}, assigned to distinct CC stretching vibrations of phenyl, central pyridyl unit or peripheral pyridyl groups [53]. Upon immersion into Cu(II) or Co(II) buffer solutions (ligand:metal molar ratio = 2:1), the SERS signal undergoes important spectral changes generating two well-discernible vibrational patterns (Fig. 3B) which can be exploited to simultaneously quantify and discriminate the two cations. In particular, major spectral alterations are clustered in the ring-breathing spectral region around 1000 cm^{-1} and, even more so, in the νC=C bands at longer wavelengths (ca. 1500-1700 cm^{-1}). Fig. 3C illustrates the normalized SERS spectra obtained at increasing Co(II) content. The 1613 and 1590 cm^{-1} features were selected as the spectral markers for free and coordinated ligands, respectively. In this case, both bands experience an overall increase in absolute intensities as the cobalt content is progressively augmented (Fig. S3). This also includes the 1590 cm^{-1} feature which one could have expected to weaken as a larger fraction of p-tpy molecules coordinates the metal cation. Such outcome can be tentatively ascribed to the resonance excitation of metal-to-ligand charge transfer transitions under 532 nm illumination (Fig. 3A). Resonance Raman condition preferentially promotes the selective enhancement of those vibrational features of the chromophore that are primarily involved in the electronic transition, which indeed includes the considered CC stretching modes of p-tpy [54]. In this case, thus, the intensity ratio I_{1613}/I_{1590} was directly used to quantitatively monitor the Co(II) concentration (Fig. 3D), yielding a linear response in the ~ 3–300 μg/L range ($r^2 = 0.996$) and a LOD of ~6 μg/L. The SERS intensity of p-tpy loaded hybrid particles remains unchanged after multiple centrifugations and washing cycles (Fig. S4), corroborating the ability of the ZIF-8 shell to efficiently entrap such ligand.

So far, we have been investigating the combination of aromatic N-heterocyclic chemoreceptors with PS@AgNP@ZIF-8 for detecting transition metal cations. Finally, to expand the range of structurally diverse potential chemoreceptors and targets, we chose Arsenazo III (AZ, Fig. 4A) as a chromogenic reagent and calcium as the target analyte. AZ is a water-soluble dye that is widely used as a reagent for the optical quantification of Ca(II) in natural waters as well as in biofluids [55]. On the other hand, calcium is a ubiquitous and very abundant alkaline earth metal for which no health-based guideline value has been proposed for drinking water. However, abnormal circulating calcium levels have been associated, among others, with neurodegenerative and cardiovascular diseases, preeclampsia, hypertension, and diabetes [56,57]. Fig. 4B shows the SERS spectra of AZ-loaded PS@AgNP@ZIF-8 particles before and after the immersion into a Ca(II) solution (200 μM). Similarly to what previously observed via conventional resonance Raman spectroscopy [58], the vibrational pattern of the SERS signal also exhibits major spectral alterations in the aromatic ring modes region (1400-1600 cm^{-1}), hinting the formation of the AZ-Ca(II) complex within the ZIF-8 network. These vibrational changes can be associated with the involvement of the azo groups together with the phenolic

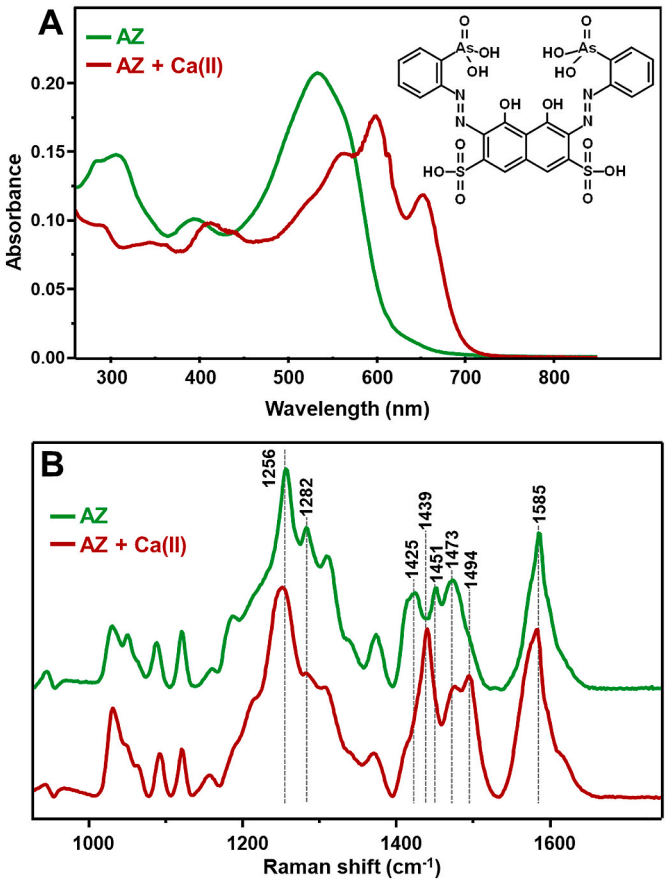

Fig. 4. (A) Absorption spectra of AZ (10 μM) and AZ + metal ions (10 μM and 20 μM, respectively) in PBS (pH 7.4). The molecular structure of AZ is also illustrated. (B) Detail of the 950-1690 cm^{-1} spectral range of the normalized SERS spectra of AZ-loaded PS@AgNPs@ZIF-8 suspension upon immersion into 200 μM Ca(II) solutions in PBS buffer (pH 7.4).

moieties in the metal coordination. It is worth noting that AZ can bind Ca(II) in several different protonated forms depending on pH [59]. No distinguishable AZ vibrational features were detected on MOF-free PS@AgNP particles at 0.1 mM chemoreceptor concentration, which further emphasizes the role of ZIF-8 in enabling the use of molecules with minimal/null affinity for metallic surfaces as efficient SERS chemoreceptors.

4. Conclusions

In summary, we demonstrated the viability of our hybrid PS@AgNPs@ZIF-8 particles to be used as a novel class of efficient and flexible SERS substrates for ultrasensitive metal ion detection in complex aqueous media. While the inner PS@AgNPs core provides a stable source of high signal magnification, the outer MOF shell firmly entraps aromatic ligands close to the plasmonic surfaces regardless of their chemical nature while retaining their properties as chromogenic reagents. Moreover, the ZIF-8 shell imparts molecular sieving abilities which enable the use of the sensing platforms in unfiltered urine samples (i.e., prefiltration steps are no longer necessary). These virtues were manifested by using various classes of molecular receptors targeting diverse metal ions as well as in the application of the sensing platform in the detection of copper in untreated urine samples for Wilson's disease diagnosis. Overall, we believe this class of multifunctional hybrid substrate will serve as a powerful material for expanding the applicability of SERS spectroscopy in real-life environmental and biomedical metal ions analysis.

Credit author statement

Nicolas Pazos-Perez: Conceptualization, Methodology, Writing – original draft. **Luca Guerrini:** Conceptualization, Methodology, Formal analysis, Resources, Writing – original draft, Supervision, Funding acquisition.

Declaration of competing interest

The authors declare that they have no known competing financial interests or personal relationships that could have appeared to influence the work reported in this paper.

Data availability

Data will be made available on request.

Acknowledgements

This research was supported by the projects PID2020-120306RB-I00 and RYC-2016-20331 (funded by MCIN/AEI), PDC2021-121787-I00 (funded by MCIN/AEI and the European Union Next Generation EU/PRTR), 2021SGR00166 (funded by Generalitat de Cataluña), 2021PFR-URV-B2-02 (funded by Universitat Rovira i Virgili).

Appendix A. Supplementary data

Supplementary data to this article can be found online at https://doi.org/10.1016/j.talanta.2023.124941.

References

[1] P.B. Tchounwou, C.G. Yedjou, A.K. Patlolla, D.J. Sutton, Heavy metal toxicity and the environment, Experientia Suppl. 101 (2012) 133–164, https://doi.org/10.1007/978-3-7643-8340-4_6.
[2] J. Dalmieda, P. Kruse, Metal cation detection in drinking water, Sensors (2019) 19, https://doi.org/10.3390/s19235134.
[3] M. Moustakas, The role of metal ions in biology, biochemistry and medicine, Materials (Basel) 14 (2021) 549, https://doi.org/10.3390/ma14030549.
[4] S. Mounicou, J. Szpunar, R. Lobinski, Metallomics: the concept and methodology, Chem. Soc. Rev. 38 (2009) 1119–1138, https://doi.org/10.1039/b713633c.
[5] L. Wang, Y.-L. Yin, X.-Z. Liu, P. Shen, Y.-G. Zheng, X.-R. Lan, C.-B. Lu, J.-Z. Wang, Current understanding of metal ions in the pathogenesis of Alzheimer's disease, Transl. Neurodegener. 9 (2020) 10, https://doi.org/10.1186/s40035-020-00189-z.
[6] E.J. Tokar, L. Benbrahim-Tallaa, M.P. Waalkes, Metal ions in human cancer development, Met. Ions Life Sci. 8 (2011) 375–401.
[7] A. Ala, A.P. Walker, K. Ashkan, J.S. Dooley, M.L. Schilsky, Wilson's disease, Lancet 369 (2007) 397–408, https://doi.org/10.1016/s0140-6736(07)60196-2.
[8] U. Merle, M. Schaefer, P. Ferenci, W. Stremmel, Clinical presentation, diagnosis and long-term outcome of Wilson's disease: a cohort study, Gut 56 (2007) 115–120, https://doi.org/10.1136/gut.2005.087262.
[9] L.H.J. Lajunen, P. Peramaki, Spectrochemical analysis by atomic absorption and emission, second ed., Royal Society of Chemistry, Cambridge, 2005.
[10] S. Botasini, G. Heijo, E. Mendez, Toward decentralized analysis of mercury (II) in real samples. A critical review on nanotechnology-based methodologies, Anal. Chim. Acta 800 (2013) 1–11, https://doi.org/10.1016/j.aca.2013.07.067.
[11] D.J. de Aberasturi, J.M. Montenegro, I.R. de Larramendi, T. Rojo, T.A. Klar, R. Alvarez-Puebla, L.M. Liz-Marzan, W.J. Parak, Optical sensing of small ions with colloidal nanoparticles, Chem. Mater. 24 (2012) 738–745, https://doi.org/10.1021/cm202380r.
[12] L. Guerrini, I. Rodriguez-Loureiro, M.A. Correa-Duarte, Y.H. Lee, X.Y. Ling, F. J. Garcia de Abajo, R.A. Alvarez-Puebla, Chemical speciation of heavy metals by surface-enhanced Raman scattering spectroscopy: identification and quantification of inorganic- and methyl-mercury in water, Nanoscale 6 (2014) 8368–8375, https://doi.org/10.1039/c4nr01464b.
[13] K.P. Carter, A.M. Young, A.E. Palmer, Fluorescent sensors for measuring metal ions in living systems, Chem. Rev. 114 (2014) 4564–4601, https://doi.org/10.1021/cr400546e.
[14] A. García-Miranda Ferrari, P. Carrington, S.J. Rowley-Neale, C.E. Banks, Recent advances in portable heavy metal electrochemical sensing platforms, Environ. Sci. 6 (2020) 2676–2690, https://doi.org/10.1039/D0EW00407C.
[15] B. Pelaz, C. Alexiou, R.A. Alvarez-Puebla, F. Alves, A.M. Andrews, S. Ashraf, L. P. Balogh, L. Ballerini, A. Bestetti, C. Brendel, S. Bosi, M. Carril, W.C.W. Chan, C. Chen, X. Chen, X. Chen, Z. Cheng, D. Cui, J. Du, C. Dullin, A. Escudero, N. Feliu, M. Gao, M. George, Y. Gogotsi, A. Grünweller, Z. Gu, N.J. Halas, N. Hampp, R. K. Hartmann, M.C. Hersam, P. Hunziker, J. Jian, X. Jiang, P. Jungebluth, P. Kadhiresan, K. Kataoka, A. Khademhosseini, J. Kopeček, N.A. Kotov, H.F. Krug, D.S. Lee, C.-M. Lehr, K.W. Leong, X.-J. Liang, M. Ling Lim, L.M. Liz-Marzán, X. Ma, P. Macchiarini, H. Meng, H. Möhwald, P. Mulvaney, A.E. Nel, S. Nie, P. Nordlander, T. Okano, J. Oliveira, T.H. Park, R.M. Penner, M. Prato, V. Puntes, V.M. Rotello, A. Samarakoon, R.E. Schaak, Y. Shen, S. Sjöqvist, A.G. Skirtach, M. G. Soliman, M.M. Stevens, H.-W. Sung, B.Z. Tang, R. Tietze, B.N. Udugama, J. S. VanEpps, T. Weil, P.S. Weiss, I. Willner, Y. Wu, L. Yang, Z. Yue, Q. Zhang, Q. Zhang, X.-E. Zhang, Y. Zhao, X. Zhou, W.J. Parak, Diverse applications of nanomedicine, ACS Nano 11 (2017) 2313–2381, https://doi.org/10.1021/acsnano.6b06040.
[16] G. Aragay, J. Pons, A. Merkoçi, Recent trends in macro-, micro-, and nanomaterial-based tools and strategies for heavy-metal detection, Chem. Rev. 111 (2011) 3433–3458, https://doi.org/10.1021/cr100383r.
[17] Y. Ding, S. Wang, J. Li, L. Chen, Nanomaterial-based optical sensors for mercury ions, TrAC, Trends Anal. Chem. 82 (2016) 175–190, https://doi.org/10.1016/j.trac.2016.05.015.
[18] S. Schlücker, Surface-enhanced Raman spectroscopy: concepts and chemical applications, Angew. Chem. Int. Ed. 53 (2014) 4756–4795, https://doi.org/10.1002/anie.201205748.
[19] J. Langer, D. Jimenez de Aberasturi, J. Aizpurua, R.A. Alvarez-Puebla, B. Auguié, J. J. Baumberg, G.C. Bazan, S.E.J. Bell, A. Boisen, A.G. Brolo, J. Choo, D. Cialla-May, V. Deckert, L. Fabris, K. Faulds, F.J. García de Abajo, R. Goodacre, D. Graham, A. J. Haes, C.L. Haynes, C. Huck, T. Itoh, M. Käll, J. Kneipp, N.A. Kotov, H. Kuang, E. C. Le Ru, H.K. Lee, J.-F. Li, X.Y. Ling, S.A. Maier, T. Mayerhöfer, M. Moskovits, K. Murakoshi, J.-M. Nam, S. Nie, Y. Ozaki, I. Pastoriza-Santos, J. Perez-Juste, J. Popp, A. Pucci, S. Reich, B. Ren, G.C. Schatz, T. Shegai, S. Schlücker, L.-L. Tay, K. G. Thomas, Z.-Q. Tian, R.P. Van Duyne, T. Vo-Dinh, Y. Wang, K.A. Willets, C. Xu, H. Xu, Y. Xu, Y.S. Yamamoto, B. Zhao, L.M. Liz-Marzán, Present and future of surface-enhanced Raman scattering, ACS Nano 14 (2020) 28–117, https://doi.org/10.1021/acsnano.9b04224.
[20] Y.Q. Wang, B. Yan, L.X. Chen, SERS tags: novel optical nanoprobes for bioanalysis, Chem. Rev. 113 (2013) 1391–1428, https://doi.org/10.1021/cr300120g.
[21] L. Jiang, M.M. Hassan, S. Ali, H. Li, R. Sheng, Q. Chen, Evolving trends in SERS-based techniques for food quality and safety: a review, Trends Food Sci. Technol. 112 (2021) 225–240, https://doi.org/10.1016/j.tifs.2021.04.006.
[22] Y.J. Hang, J. Boryczka, N.Q. Wu, Visible-light and near-infrared fluorescence and surface-enhanced Raman scattering point-of-care sensing and bio-imaging: a review, Chem. Soc. Rev. 51 (2022) 329–375, https://doi.org/10.1039/c9cs00621d.
[23] J. Choi, J.H. Kim, J.W. Oh, J.M. Nam, Surface-enhanced Raman scattering-based detection of hazardous chemicals in various phases and matrices with plasmonic nanostructures, Nanoscale 11 (2019) 20379–20391, https://doi.org/10.1039/c9nr07439b.
[24] M. Li, H. Gou, I. Al-Ogaidi, N. Wu, Nanostructured sensors for detection of heavy metals: a review, ACS Sustain. Chem. Eng. 1 (2013) 713–723, https://doi.org/10.1021/sc400019a.
[25] L. Guerrini, R.A. Alvarez-Puebla, Surface-enhanced Raman scattering sensing of transition metal ions in waters, ACS Omega 6 (2021) 1054–1063, https://doi.org/10.1021/acsomega.0c05261.
[26] W. Ji, L. Li, Y. Zhang, X. Wang, Y. Ozaki, Recent advances in surface-enhanced Raman scattering-based sensors for the detection of inorganic ions: sensing mechanism and beyond, J. Raman Spectrosc. 52 (2021) 468–481, https://doi.org/10.1002/jrs.5975.
[27] W.F. Zhu, J.A. Hutchison, M.D. Dong, M. Li, Frequency shift surface-enhanced Raman spectroscopy sensing: an ultrasensitive multiplex assay for biomarkers in human health, ACS Sens. 6 (2021) 1704–1716, https://doi.org/10.1021/acssensors.1c00393.
[28] Z. Duan, X. Zhang, T. Ye, X. Zhang, S. Dong, J. Liu, X. Xiao, C. Jiang, Ultrasensitive Au nanooctahedron micropinball sensor for mercury ions, ACS Appl. Mater. Interfaces 10 (2018) 25737–25743, https://doi.org/10.1021/acsami.8b04414.
[29] Y. Shi, N. Chen, Y. Su, H. Wang, Y. He, Silicon nanohybrid-based SERS chips armed with an internal standard for broad-range, sensitive and reproducible simultaneous quantification of lead(II) and mercury(II) in real systems, Nanoscale 10 (2018) 4010–4018, https://doi.org/10.1039/c7nr07935d.
[30] L. Guerrini, R.A. Alvarez-Puebla, Multiplex SERS chemosensing of metal ions via DNA-mediated recognition, Anal. Chem. 91 (2019) 11778–11784, https://doi.org/10.1021/acs.analchem.9b02385.
[31] C. Koh, O. Sim, S.X. Leong, S.K. Boong, C.R.C. Chong, X.Y. Ling, Plasmonic nanoparticle-metal-organic framework (NP-MOF) nanohybrid platforms for emerging plasmonic applications, ACS Mater. Lett. 3 (2021) 557–573, https://doi.org/10.1021/acsmaterialslett.1c00047.
[32] P.X. Wang, Y. Sun, X. Li, L. Wang, Y. Xu, G.L. Li, Recent advances in metal organic frameworks based surface enhanced Raman scattering substrates: synthesis and applications, Molecules 26 (2021), https://doi.org/10.3390/molecules26010209.
[33] H.S. Lai, G.K. Li, F.G. Xu, Z.M. Zhang, Metal-organic frameworks: opportunities and challenges for surface-enhanced Raman scattering - a review, J. Mater. Chem. C 8 (2020) 2952–2963, https://doi.org/10.1039/d0tc00040j.
[34] C. Carrillo-Carrion, R. Martinez, M.F. Navarro Poupard, B. Pelaz, E. Polo, A. Arenas-Vivo, A. Olgiati, P. Taboada, M.G. Soliman, U. Catalan, S. Fernandez-Castillejo, R. Sola, W.J. Parak, P. Horcajada, R.A. Alvarez-Puebla, P. Del Pino, Aqueous stable gold nanostar/ZIF-8 nanocomposites for light-triggered release of active cargo inside living cells, Angew. Chem. Int. Ed. 58 (2019) 7078–7082, https://doi.org/10.1002/anie.201902817.
[35] G.C. Phan-Quang, N. Yang, H.K. Lee, H.Y.F. Sim, C.S.L. Koh, Y.C. Kao, Z.C. Wong, E.K.M. Tan, Y.E. Miao, W. Fan, T. Liu, I.Y. Phang, X.Y. Ling, Tracking airborne molecules from Afar: three-dimensional metal-organic framework-surface-

enhanced Raman scattering platform for stand-off and real-time atmospheric monitoring, ACS Nano 13 (2019) 12090–12099, https://doi.org/10.1021/acsnano.9b06486.
[36] C.H. Huang, A.L. Li, X.Y. Chen, T. Wang, Understanding the role of metal-organic frameworks in surface-enhanced Raman scattering application, Small 16 (2020), https://doi.org/10.1002/smll.202004802.
[37] H.Y.F. Sim, H.K. Lee, X. Han, C.S.L. Koh, G.C. Phan-Quang, C.L. Lay, Y.C. Kao, I. Y. Phang, E.K.L. Yeow, X.Y. Ling, Concentrating immiscible molecules at solid@MOF interfacial nanocavities to drive an inert gas-liquid reaction at ambient conditions, Angew. Chem. Int. Ed. 57 (2018) 17058–17062, https://doi.org/10.1002/anie.201809813.
[38] C.S.L. Koh, H.K. Lee, X. Han, H.Y.F. Sim, X.Y. Ling, Plasmonic nose: integrating the MOF-enabled molecular preconcentration effect with a plasmonic array for recognition of molecular-level volatile organic compounds, Chem. Commun. 54 (2018) 2546–2549, https://doi.org/10.1039/C8CC00564H.
[39] X.R. Deng, S. Liang, X.C. Cai, S.S. Huang, Z.Y. Cheng, Y.S. Shi, M.L. Pang, P.A. Ma, J. Lin, Yolk-shell structured au nanostar@metal-organic framework for synergistic chemo-photothermal therapy in the second near-infrared window, Nano Lett. 19 (2019) 6772–6780, https://doi.org/10.1021/acs.nanolett.9b01716.
[40] T. Zorlu, B. Puértolas, I.B. Becerril-Castro, V. Giannini, M.A. Correa-Duarte, R. A. Alvarez-Puebla, Optical quantification of metal ions using plasmonic nanostructured microbeads coated with metal–organic frameworks and ion-selective dyes, ACS Nanosci. Au 3 (2023) 222–229, https://doi.org/10.1021/acsnanoscienceau.2c00063.
[41] L.M. Sayre, G. Multhaup, Alzheimer's precursor protein and the use of bathocuproine for determining reduction of copper(II), Science 274 (1996) 1933–1934, https://doi.org/10.1126/science.274.5294.1933.
[42] H. Diehl, F.G. Smith, The Copper Reagents: Cuproine, Neocuproine, Bathocuproine, The G. Frederick Smith Chemical Company, Columbus, Ohio (US), 1958.
[43] N. Pazos-Perez, J.M. Fitzgerald, V. Giannini, L. Guerrini, R.A. Alvarez-Puebla, Modular assembly of plasmonic core–satellite structures as highly brilliant SERS-encoded nanoparticles, Nanoscale Adv. 1 (2019) 122–131, https://doi.org/10.1039/C8NA00257F.
[44] S. Chen, X.-Y. Liu, J. Jin, M. Gao, C. Chen, Q. Kong, Z. Ji, G.A. Somorjai, O. M. Yaghi, P. Yang, Individually encapsulated frame-in-frame structure, ACS Mater. Lett. 2 (2020) 685–690, https://doi.org/10.1021/acsmaterialslett.0c00161.
[45] C. Wei, Y. He, X. Shi, Z. Song, Terpyridine-metal complexes: applications in catalysis and supramolecular chemistry, Coord. Chem. Rev. 385 (2019) 1–19, https://doi.org/10.1016/j.ccr.2019.01.005.
[46] E. V Solovyeva, A. Rakhimbekova, Y. V Lanchuk, L.A. Myund, A.S. Denisova, SERS investigation of neocuproine adsorption on silver: influence of electrode potential on methyl groups, J. Raman Spectrosc. 49 (2018) 207–214, https://doi.org/10.1002/jrs.5265.
[47] A. Lucena-Valera, D. Perez-Palacios, R. Muñoz-Hernandez, M. Romero-Gómez, J. Ampuero, Wilson's disease: revisiting an old friend, World J. Hepatol. 13 (2021) 634–649, https://doi.org/10.4254/wjh.v13.i6.634.
[48] T. Ueda, T. Yamatani, M. Okumura, Dynamic gate opening of ZIF-8 for bulky molecule adsorption as studied by vapor adsorption measurements and computational approach, J. Phys. Chem. C 123 (2019) 27542–27553, https://doi.org/10.1021/acs.jpcc.9b07239.
[49] G. Zheng, S. de Marchi, V. López-Puente, K. Sentosun, L. Polavarapu, I. Pérez-Juste, E.H. Hill, S. Bals, L.M. Liz-Marzán, I. Pastoriza-Santos, J. Pérez-Juste, Encapsulation of single plasmonic nanoparticles within ZIF-8 and SERS analysis of the MOF flexibility, Small 12 (2016) 3935–3943, https://doi.org/10.1002/smll.201600947.
[50] E.C. Constable, 2,2':6',2''-terpyridines: from chemical obscurity to common supramolecular motifs, Chem. Soc. Rev. 36 (2007) 246–253, https://doi.org/10.1039/b601166g.
[51] D. Tsoutsi, L. Guerrini, J.M. Hermida-Ramon, V. Giannini, L.M. Liz-Marzan, A. Wei, R.A. Alvarez-Puebla, Simultaneous SERS detection of copper and cobalt at ultratrace levels, Nanoscale 5 (2013) 5841–5846, https://doi.org/10.1039/c3nr01518a.
[52] U. Siemeling, J.V. der Brüggen, U. Vorfeld, A. Stammler, H.-G. Stammler, Large Scale Synthesis of 4'-(4-Bromophenyl)-2,2':6',2"-terpyridine and nature of the mysterious green by-product, Z. Naturforsch. B Chem. Sci. 58 (2003) 443–446, https://doi.org/10.1515/znb-2003-0514.
[53] A.P. Mangoni, B. Brandao, J.S. Shinohara, A.T. Silveira, M. Nakamura, H.E. Toma, Raman studies of bis(phenylterpyrazine)iron(II) and supramolecular species with pentacyanidoferrate(II) ions, Quim. Nova 42 (2019) 1020–1028, https://doi.org/10.21577/0100-4042.20170415.
[54] J. Kozisek, J. Svoboda, J. Zednik, B. Vlckova, I. Sloufova, Resonance Raman excitation profiles of Fe(II)-terpyridine complexes: electronic effects of ligand modifications, J. Phys. Chem. B 125 (2021) 12847–12858, https://doi.org/10.1021/acs.jpcb.1c08366.
[55] N.O. Leary, A. Pembroke, P.F. Duggan, Single stable reagent (arsenazo III) for optically robust measurement of calcium in serum and plasma, Clin. Chem. 38 (1992) 904–908, https://doi.org/10.1093/clinchem/38.6.904.
[56] G.R. Monteith, D. McAndrew, H.M. Faddy, S.J. Roberts-Thomson, Calcium and cancer: targeting Ca^{2+} transport, Nat. Rev. Cancer 7 (2007) 519–530, https://doi.org/10.1038/nrc2171.
[57] S. Xu, M. Zhang, J. Cong, Y. He, L. Zhang, Y. Guo, X. Li, Reduced blood circulating calcium level is an outstanding biomarker for preeclampsia among 48 types of human diseases, QJM, 2021, https://doi.org/10.1093/qjmed/hcab222.
[58] B. Ehrenberg, Arsenazo III, a resonance Raman indicator with high selectivity for Ca^{2+}, FEBS Lett. 140 (1982) 219–222, https://doi.org/10.1016/0014-5793(82)80898-3.
[59] V.C.K. Chiu, D. Haynes, The pH dependence and the binding equilibria of the calcium indicator - arsenazo III, Membr. Biochem. 3 (1980) 169–183, https://doi.org/10.3109/09687688009063884.